THE JOURNAL OF BIOLOGICAL CHEMISTRY
Vol. 280, No. 9, Issue of March 4, pp. 8060–8068, 2005
Printed in U.S.A.

The Molecular Mechanisms of Coactivator Utilization in Ligand-dependent Transactivation by the Androgen Receptor*[S]

Received for publication, June 23, 2004, and in revised form, November 2, 2004
Published, JBC Papers in Press, November 24, 2004, DOI 10.1074/jbc.M407046200

Eva Estébanez-Perpiñá‡, Jamie M. R. Moore§, Ellena Mar‡, Edson Delgado-Rodrigues¶, Phuong Nguyen¶, John D. Baxter¶‖, Benjamin M. Buehrer‡‡, Paul Webb¶, Robert J. Fletterick‡, and R. Kiplin Guy§ §§**

*From the ‡Department of Biochemistry and Biophysics, University of California, San Francisco, California 94143, the §Departments of Pharmaceutical Chemistry and Cellular and Molecular Pharmacology, University of California, San Francisco, California 94143, the ¶Metabolic Research Unit and Diabetes Center, University of California, San Francisco, California 94143, and **Karo Bio USA, Durham, North Carolina 27703*

Androgens drive sex differentiation, bone and muscle development, and promote growth of hormone-dependent cancers by binding the nuclear androgen receptor (AR), which recruits coactivators to responsive genes. Most nuclear receptors recruit steroid receptor coactivators (SRCs) to their ligand binding domain (LBD) using a leucine-rich motif (L*XX*LL). AR is believed to recruit unique coactivators to its LBD using an aromatic-rich motif (F*XX*LF) while recruiting SRCs to its N-terminal domain (NTD) through an alternate mechanism. Here, we report that the AR-LBD interacts with both F*XX*LF motifs and a subset of L*XX*LL motifs and that contacts with these L*XX*LL motifs are both necessary and sufficient for SRC-mediated AR regulation of transcription. Crystal structures of the activated AR in complex with both recruitment motifs reveal that side chains unique to the AR-LBD rearrange to bind either the bulky F*XX*LF motifs or the more compact L*XX*LL motifs and that AR utilizes subsidiary contacts with L*XX*LL flanking sequences to discriminate between L*XX*LL motifs.

The cellular effects of the hormone 5-α-dihydrotestosterone (DHT)[1] are mediated by the androgen receptor (AR), a member of the nuclear hormone receptor superfamily (1). AR is absolutely required for normal male development, plays a variety of important roles in metabolism and homeostasis in adult men and women (2, 3), and is required for prostate cancer growth. Consequently, AR is a major target for pharmaceutical development and the recognized target for existing prostate cancer therapies, including androgen withdrawal and antiandrogens (1, 4–6). It is nonetheless desirable to obtain new antiandrogens that spare patients from harmful side-effects and inhibit AR action in secondary hormone-resistant prostate cancer, where AR action becomes sensitized to low levels of androgens or existing antiandrogens (6, 7). Improved understanding of AR signaling pathways will facilitate development of these compounds.

Like most nuclear receptors (NRs), AR activity depends on interactions with members of the steroid receptor coactivator (SRC) family (1, 8, 9). Several lines of evidence indicate that AR contacts with SRCs are important in prostate cancer. First, androgens promote SRC recruitment to the androgen-regulated prostate-specific antigen promoter, and this event is inhibited by the antiandrogen flutamide (10). Second, exogenous SRC2 (GRIP1/TIF2) promotes the androgen-dependent progression from the G_1 to S phase in LNCaP prostate tumor cells, in a manner that requires specific AR contact (10). Third, SRCs often become expressed at high levels in prostate cancers (5). Finally, AR contacts with SRCs mediate hormone-independent AR signaling in conditions that resemble secondary prostate cancer (11, 12). Thus, strategies to inhibit AR contacts with SRCs could be useful in blocking prostate cancer cell growth.

For many NRs, overall transcriptional activity stems mostly from the hormone-dependent activation function (AF-2) within the NRs ligand binding domain (LBD), and involves interaction between a conserved hydrophobic cleft on the surface of the LBD and short leucine-rich hydrophobic motifs (NR boxes, consensus L*XX*LL motif) reiterated within each SRC (13, 14). In contrast, current models of AR action suggest that AR activity stems from a potent hormone-independent activation function, AF-1, within the N-terminal domain (NTD) of the AR and emphasize the role of contacts between NTD and glutamine-rich sequences within the SRC C terminus in SRC recruitment (15–19). The AR-LBD is proposed to bind L*XX*LL motifs weakly and, instead, bind preferentially to aromatic-rich motifs that are found within the AR NTD (FQNLF and WHTLF) and AR-specific coactivators such as ARA70 (16, 20–23). The intramolecular interactions between the LBD and the

* This work was supported by the Prostate Cancer Foundation, by National Institutes of Health Grants DK58080 (to R. J. F. and R. K. G.) DK51281 (to J. D. B.), and CA8952 (to E. E.-P.) and by Department of Defense Grants DAMD17-01-1-0188 (to J. M. R. M.) and PC030607 (to P. W.). The costs of publication of this article were defrayed in part by the payment of page charges. This article must therefore be hereby marked "*advertisement*" in accordance with 18 U.S.C. Section 1734 solely to indicate this fact.

The atomic coordinates and structure factors (codes 1T63, 1T5Z, 1T65, and 1XJ7) have been deposited in the Protein Data Bank, Research Collaboratory for Structural Bioinformatics, Rutgers University, New Brunswick, NJ (http://www.rcsb.org/).

[S] The on-line version of this article (available at http://www.jbc.org) contains supplemental Fig. SI.

‖ Has proprietary interests in, and serves as a consultant and Deputy Director to, Karo Bio AB, which has commercial interests in this area of research.

‡‡ Present address, Karo Bio AB, Halsovagen, S-141, 57 Huddinge, Sweden.

§§ To whom correspondence should be addressed: Dept. of Pharmaceutical Chemistry, University of California, 600 16th St., San Francisco, CA 94143. Tel.: 415-502-7051; Fax: 415-514-0689; E-mail: rguy@cgl.ucsf.edu.

[1] The abbreviations used are: DHT, 5-α-dihydrotestosterone; AR, androgen receptor; NR, nuclear receptor; Fmoc, *N*-(9-fluorenyl)methoxycarbonyl; SRC, steroid receptor coactivator; LBD, ligand binding domain; NTD, N-terminal domain; MMTV, mouse mammary tumor virus; LTR, long terminal repeat; GST, glutathione *S*-transferase; DBD, DNA binding domain; CMV, cytomegalovirus; TR, thyroid receptor; AF, activation function.

NTD FQNLF motif promote formation of head to tail dimers (N-C interaction), which render the AF-2 surface unavailable for direct cofactor contacts (21). Together, the notion that AR AF-2 binds coactivators weakly, and the fact that it will be occluded by the N-C interaction, has led to the suggestion that AR AF-2 does not play an active role in SRC recruitment.

Nonetheless, several lines of evidence suggest that AR AF-2 can contribute directly to coactivator recruitment in some contexts. First, the N-C interaction is required for optimal AR activity at some promoters, including those of *probasin*, *prostate-specific antigen*, and *C3*, but not at others, including those of the *sex-limiting protein* and the mouse mammary tumor virus-long terminal repeats (MMTV-LTRs) (16). Thus, AF-2 may be available for coactivator contacts in some circumstances. Second, mutation of AR AF-2 recognition sequences within target coactivators inhibits AR coactivation (16, 19, 20). Thus, mutation of F*XX*LF motifs within AR-specific coactivators such as ARA70 blocks their ability to interact with AR and potentiate AF-2 activity. More surprisingly, given the prevailing notion that AR AF-2 contacts with L*XX*LL motifs are weak, mutation of all three SRC L*XX*LL motifs inhibits AR coactivation when SRCs are overexpressed, when AR NTD FQNLF and WHTLF motifs are mutated, or when AR acts at promoters such as the MMTV-LTR.

It is important to understand the overall significance of particular AR to coregulator contacts, and the mechanism of these interactions, to develop strategies to inhibit AR activity in prostate cancer. In this study, we examine AR AF-2 interactions with target coactivators. Our studies confirm that AR AF-2 binds F*XX*LF motifs, but also show that AR AF-2 binds a subset of SRC L*XX*LL motifs with higher affinity and, further, that the same L*XX*LL motifs are required to mediate AR AF-2 activity. Crystal structures of AR-LBD in complex with native F*XX*LF and L*XX*LL peptides reveal the structural basis for these unusual coactivator binding preferences and may suggest new approaches to drug design.

EXPERIMENTAL PROCEDURES

Protein Expression and Purification—AR-LBD (residues 663–919) was expressed in *Escherichia coli* and purified to homogeneity using a modified version of previously published protocols (24). Bacterial cell preparations were grown at ambient or lower temperatures to high optical density at 600 nm (>1.00) in 2× LB supplemented with DHT. AR-LBD protein was expressed by induction with isopropyl 1-thio-β-D-galactopyranoside for 14–16 h at 15 °C before harvest and cell lysis by freeze-thawing and mild sonication. Purification involved an initial affinity chromatography step using a glutathione-Sepharose column, followed by thrombin cleavage of the GST affinity tag. Finally cation exchange chromatography with Sepharose SP afforded the purified protein. Our procedures differ from published work in that we use Sepharose SP for the second purification step instead of Fractogel SO_3, which does not retain AR in our experiments.

Peptide Library Synthesis—Coregulator peptides consisting of 20 amino acids with the general motif of **C***XXXXXXX***LXX**(**L/A**)(**L/A**)*XXXXXXX* were constructed, where C is cysteine, L is leucine, A is alanine, and *X* is any amino acid. The sequences of all the coregulator peptides were obtained from human isoform candidate genes (SRC1/AAC50305, SRC2/Q15596, SRC3/Q9Y6Q9, and ARA70/Q13772). The peptides were synthesized in parallel using standard Fmoc chemistry in 48-well synthesis blocks (FlexChem System, Robbins). Preloaded Wang (Novagen) resin was deprotected with 20% piperidine in dimethylformamide. The next amino acid was then coupled using 2-(1H-benzotriazole-1-yl)-1,1,3,3-tetramethyluronium hexafluorophosphate (2.38 eq. wt.), Fmoc-protected amino acid (2.5 eq. wt.), and diisopropylethylamine (5 eq. wt.) in anhydrous dimethylformamide. Coupling efficiency was monitored by the Kaiser test. Synthesis then proceeded through a cycle of deprotection and coupling steps until the peptides were completely synthesized. The completed peptides were cleaved from the resin with concomitant side-chain deprotection (81% trifluoroacetic acid, 5% phenol, 5% thioanisole, 2.5% ethanedithiol, 3% water, 2% dimethylsulfide, 1.5% ammonium iodide), and crude product was dried down using a SpeedVac (GeneVac). Reversed-phase chromatography followed by mass spectrometry (matrix-assisted laser desorption ionization time-of-flight/electrospray ionization) was used to purify the peptides. The purified peptides were then lyophilized. A thiol-reactive fluorophore, 5-iodoacetamidofluorescein (Molecular Probes), was then coupled to the N-terminal cysteine following the manufacturer's protocol. Labeled peptide was isolated using reversed-phase chromatography and mass spectrometry. Peptides were quantified using UV spectroscopy. Purity was assessed using liquid chromatography/mass spectrometry.

Peptide Binding Assay—Using a BiomekFX in the Center for Advanced Technology, AR-LBD was serially diluted from 100 μM to 0.002 μM in binding buffer (50 mM sodium phosphate, 150 mM NaCl, pH 7.2, 1 mM dithiothreitol, 1 mM EDTA, 0.01% Nonidet P-40, 10% glycerol) containing 150 μM ligand (dihydroxytestosterone) in 96-well plates. Then 10 μl of diluted protein was added to 10 μl of fluorescent coregulator peptide (20 nM) in 384-well plates yielding final protein concentrations of 50–0.001 μM and 10 nM fluorescent peptide concentration. The samples were allowed to equilibrate for 30 min. Binding was then measured using fluorescence polarization (excitation λ, 485 nm; emission λ, 530 nm) on an Analyst AD plate reader (Molecular Devices). Two independent experiments were assayed for each state in quadruplicate. Data were analyzed using SigmaPlot 8.0 (SPSS, Chicago, IL), and the K_d values were obtained by fitting data to the equation, $y = \min + (\max - \min)/1 + (x/K_d)\wedge\text{Hillslope}$.

GST Pull-down Assays—Full-length SRC-2 (amino acids 1–1462) and AR NTD-DBD (amino acids 1–660) was expressed in a coupled transcription/translation system (TNT, Promega). AR-LBD (amino acids 646–919), or AR-LBD mutants, were expressed in *E. coli* strain BL21 as a GST fusion protein and attached to glutathione beads according to the manufacturer's protocol (Amersham Biosciences). Binding assays were performed by mixing glutathione-linked Sepharose beads containing 4 μg of GST fusion protein (estimated by Coomassie Plus protein assay reagent, Pierce) with 2 μl of ^{35}S-labeled SRC-2 or AR NTD-DBD in 20 mM HEPES, 150 mM KCl, 25 mM $MgCl_2$, 10% glycerol, 1 mM dithiothreitol, 0.2 mM phenylmethylsulfonyl fluoride, 20 μg/ml bovine serum albumin, and protease inhibitors containing to a final volume of 150 μl. The bead mix was shaken at 4 °C for 1.5 h, washed three times in 200 μl of binding buffer. The bound proteins were resuspended in SDS-PAGE loading buffer, separated by using 10% SDS-polyacrylamide gel electrophoresis, and visualized by autoradiography.

Cell Culture and Transfection Assays—HeLa, DU145, and CV-1 cells were maintained in Dulbecco's modified Eagle's medium H-21 4.5 g/liter glucose, containing 10% steroid depleted fetal bovine serum (Invitrogen), 2 mM glutamine, 50 units/ml penicillin, and 50 mg/ml streptomycin. For transfection, cells were collected and resuspended in Dulbecco's phosphate-buffered saline (0.5 ml/4.5 × 10^7 cells) containing 0.1% dextrose, and typically 4 μg of luciferase reporter plasmid, 1 μg of AR expression vector or empty vector control, and 2 μg of pCMV-β-galactosidase. Cells were electroporated at 240 V and 960 microfarads, transferred to fresh media, and plated into 12-well plates. After incubation for 24 h at 37 °C with androgen or vehicle, cells were collected, and pellets were lysed by addition of 150 μl of 100 mM Tris-HCl, pH 7.8, containing 0.1% Triton X-100.

For transfections with full-length AR, the reporter gene utilized the Mouse Mammary Tumor Virus promoter fused to luciferase. For transfections with *GAL-AR-LBD*, *GAL-TR LBD*, and *GAL-CBP* fusions, the reporter contained five *GAL4* response elements upstream of a minimal promoter. LUC and β-galactosidase activities were measured using the Luciferase Assay System (Promega) and Galacto-Light Plus β-galactosidase reporter gene assay system (Applied Biosystems), according to the manufacturer's instructions.

Crystallization, Structure Determination, and Refinement—The complexes of SRC2–2, SRC2–3, SRC3–2, and ARA70 peptides and AR-LBD were prepared by mixing at 0 °C for 2 h, with variable ratios of peptide (3–10 mM) and protein (at about 4.5 mg/ml). Crystals were obtained by vapor diffusion methods (sitting-drop technique) using crystal screens from Hampton. The protein-peptide complex solution was mixed with the reservoir solution (0.8 M sodium citrate, 0.1 M Tris, pH 7.5 or pH 8.0), and concentrated against 300 μl of the reservoir. Crystals appeared after 1 day and grew to maximal dimensions after 4 days. After 4 days these crystals started to crack, so new crystallization trials were necessary to find additives that would stabilize the crystals. 0.3 μl of either 2.0 M NaCl, 1.0 M $LiCl_2$, or 0.1 M EDTA were added to a 1-μl protein plus a −1-μl reservoir drop to stabilize AR-LBD crystals at room temperature.

Crystals for either AR-DHT or AR-DHT-peptide were transferred to a new drop containing 10% (v/v) of glycerol for cryoprotection. The crystals were then flash-cooled using liquid nitrogen and measured

TABLE I
Statistics for data collection and refinement

	AR-SRC2–3	AR-SRC2–2 (non-helical)	AR-SRC3 (RAC3)	AR-ARA70
Molecules/asymmetric unit	1	1	1	1
Space group	$P2_12_12_1$	$P2_12_12_1$	$P2_12_12_1$	$P2_12_12_1$
Cell constants a/b/c (Å)	54.49/67.37/70.52	55.60/67.58/69.32	53.06/66.83/71.07	55.68/66.42/68.25
Resolution (Å)	2.07	1.66	2.7	2.3
Reflections measured	393,765	511,617	375,686	458,173
Unique reflections	16,416	35,221	17,753	13,713
Overall completeness (%)	97.2	91.7	90	92.8
Outermost shell completeness (%)	94.3	88.0	83.8	85.2
R merge (%)[a]	4.4	6	5.5	5
Reflections used refinement	15,915	32,260	6,151	10,881
Resolution range (Å)	24–2.07	25–1.66	25–2.7	24–2.3
R factor (%)[b]	19.8	21.1	25.3	22.8
R free (%)[c]	23.2	24.8	31.5	25.8
Number of water molecules	160	361	100	106
Matthews coefficient	2.157	2.116	2.100	2.104
Solvent content (%)	43	42	41.5	40
Ramachandran plot most favored (%)	93	92	82	92
Ramachandran plot allowed (%)	7	7	17	8

[a] R merge (%) = $\Sigma_{hkl}|\langle I\rangle - I|/\Sigma_{hkl}|I|$.
[b] R factor (%) = $\Sigma_{hkl}||F_o| - |F_c||/\Sigma_{hkl}|F_o|$.
[c] The R free set contained 5% of total data.

using the synchrotron radiation at the 8.3.1 beam line at the Advanced Light Source (Berkeley). Crystals containing SRC2-3, SRC2-2, and SRC3-2 diffracted to 2.07, 1.66, and 2.7 Å, respectively. Cocrystals of ARA70 peptide with AR-LBD were also grown, and a complete data set was obtained at 2.3 Å resolution. All the crystals belong to space group $P2_12_12_1$ (orthorhombic) and contain one molecule per asymmetric unit.

The diffraction data were integrated and scaled using the computer program ELVES (ucxray.berkeley.edu/~jamesh/elves/) (25). Molecular replacement solutions for all AR-LBD peptide structures were obtained using rotation and translation functions from Crystallography & NMR Systems (CNS, cns.csb.yale.edu/v1.1/) (26).

The first electron maps calculated after the rigid body refinement that followed the molecular replacement displayed clear electron density for the peptides. During the improvement of the protein model, the Fourier maps revealed better electron density for more flanking residues of the peptides. The electron density for the peptide was always modeled as a short α-helix. However, refinement of the SRC2-2 peptide as an α-helix was unsuccessful as such peptide does not adopt such helical conformation on the AR-LBD AF2 surface. Further SRC2-2 model building and refinement were not pursued as an α-helix. A composite omit map not including the peptides was calculated in the last steps of refinement for overcoming phase bias for each one of the complexes. This map was calculated omitting 5% of the total model allowing a better tracing of the peptide and permitted to visualize more residues that were not visible in the $2F_o - F_c$ map. Model building was done using the program QUANTA (Accelrys Software, www.accelrys.com/quanta/) monitored using the free R factor. Calculation of the electron density maps and crystallographic refinement was performed with CNS using the target parameters of Engh and Huber (27). Several cycles of model building, conjugate gradient minimization, and simulated annealing using CNS resulted in structures with good stereochemistry. A Ramachandran plot shows that most of the residues fall into the most favored or additionally favored regions. The statistics for data collection and refinement of each one of the data sets can be found in Table I.

The structures have been deposited with the Protein Data Bank (PDB) and assigned the following ID numbers: AR·DHT·SRC2-3, PDB 1T63, RCSB RCSB022358; AR·DHT·ARA70, PDB 1T5Z, RCSB RCSB022354; AR·DHT·SRC2-2, PDB 1T65, RCSB RCSB022360; and AR·DHT·SRC3-2, PDB 1XJ7, RCSB RCSB030414.

RESULTS

AR AF-2 Binds SRC-2 NR Boxes 1 and 3 with High Affinity—To understand the unusual spectrum of AR AF-2 coactivator interactions, we measured binding of the AR-LBD to a library composed of NR boxes from known coactivating proteins, including both SRCs and AR specific coactivators (Fig. 1*A*). Such peptides are known to bind to other NRs with equal affinity to the full-length coactivator (28). AR-LBD interacted to varying degrees with all of the peptides containing an L*XX*LL motif tested except the first NR box of ARA70. As expected, AR-LBD interacted with F*XX*LF sequences present in ARA70 and the AR NTD (21, 29) fairly strongly with measurable dissociation constants of 33 ± 3.3 and 38 ± 3.8 μM, respectively. Surprisingly, AR also recognized a subset of NR boxes from the SRC family (30). Specifically, peptides of the first (SRC2-1, K_d = 13 ± 2.1 μM) and third (SRC2-3, K_d = 15 ± 1.2 μM) NR boxes of SRC-2 (GRIP1/TiF-2/N-CoA-2) bound strongly to AR, followed in affinity by F*XX*LF motifs. The second NR box of SRC3 (RAC3/p/CIP/p300/CBP-interacting protein) was also recruited to AR (K_d = 39 ± 5 μM). The remaining NR boxes from SRC-1, SRC-2, and NTD weakly interacted with AR either nonspecifically or with binding affinities above the assay range (>40 μM). Control experiments with the same sequences in which L*XX*LL or F*XX*LF had been converted to L*XX*AA or F*XX*AA revealed the binding was dependent upon the intact triad of hydrophobic amino acids (not shown). This substitution has been shown previously to abolish interactions with NR (31).

Pull-down experiments confirmed that the AR-LBD bound SRC2 strongly, as opposed to the AR NTD or NTD-DBD (Fig. 1*B*). Furthermore, AR-LBD interactions with SRC2 were inhibited by mutation of SRC2 boxes 2 and 3 (Fig. 1*C*), or by increasing concentrations of SRC2-3 peptide (Fig. 1*D*). Thus, AR-LBD binds F*XX*LF motifs but also binds a subset of classic NR box peptides with comparable or higher affinities. Moreover, the preference of AR for individual L*XX*LL motifs is different from that observed with other NRs, such as the estrogen receptor and thyroid receptors (TRs), which bind box 2 in each of the three SRCs with high affinity (28, 32–34).

AR-dependent Transactivation Requires SRC2 Boxes 1 and 3—Next, we examined the ability of SRC2 to coactivate isolated AR AF-2 and requirements for individual L*XX*LL motifs in this effect. As expected, a fusion protein containing the AR-LBD (amino acids 646–919) linked to the yeast GAL4 DNA binding function conferred androgen-dependent transcriptional activity on a GAL4-responsive reporter in several cell types, and simultaneous expression of SRC2 strongly enhanced AR AF-2 activity (Fig. 2*A*). Overall, AR AF-2 activity was more potent than that of AR AF-1 in HeLa and DU145, particularly in the presence of SRC2, and about 20–30% as potent as that induced by TR and estrogen receptorα LBDs, which bind a wider range of SRCs (see supplemental material). As expected from prior results, AF-1 dominates signaling in CV-1 cells, the effects of

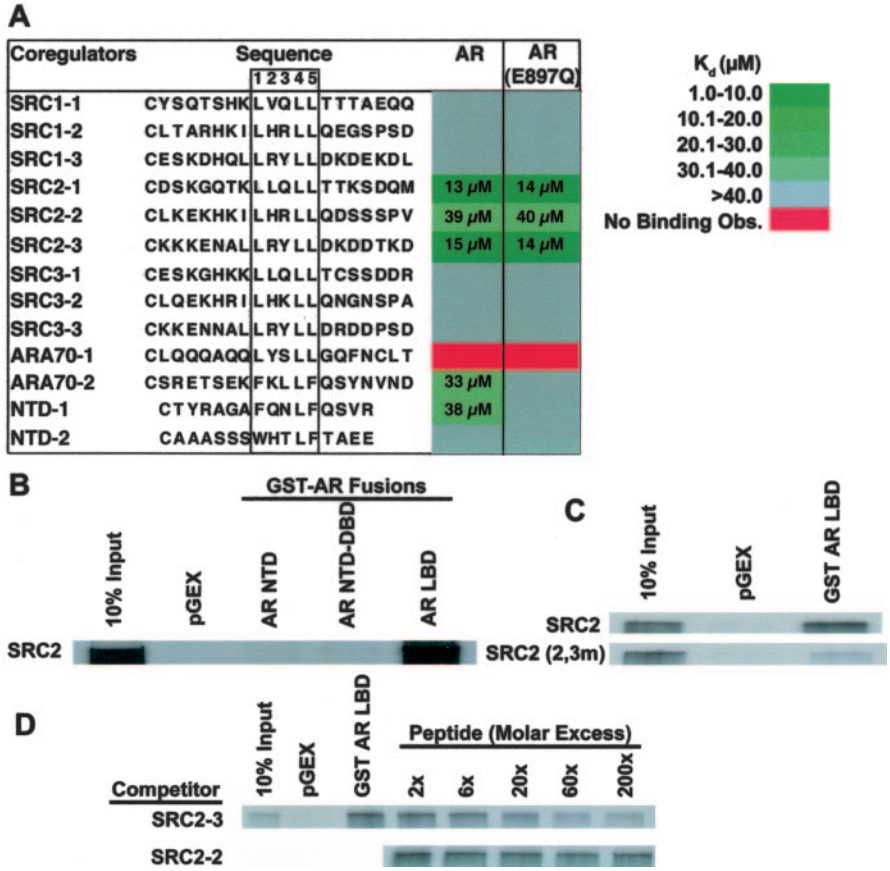

FIG. 1. **The androgen receptor-ligand binding domain (*AR-LBD*) binds a subset of steroid receptor coactivator (*SRC*) nuclear receptor interaction motifs (NR boxes).** *A*, sequences of relevant NR boxes and relative equilibrium affinities of these NR boxes for binding to AR-LBD and a mutant AR-LBD (E897Q) in which one charge clamp residue has been neutralized. The binding affinities were determined using fluorescence polarization with fluorescently labeled NR box peptides. The coregulator peptides are listed in the *left column* where *SRC1-1*, *SRC1-2*, and *SRC1-3* represent the first, second, and third NR boxes in SRC1, respectively. Each *color* represents a unique K_d range as defined by the legend in the *bottom right-hand corner*. For coregulator peptides that displayed saturated binding curves with AR, the actual K_d values are listed. The *gray color* represents conditions where some interaction of coregulator peptides with AR was observed, however, saturating binding curves were not achieved in the protein concentration range studied. *B*, pull down of SRC2 by GST fusions of AR domains. *C*, effects of mutation of NR boxes of SRC2 on the pull down by the GST fusion of the AR-LBD. *SRC2 (2,3m)* indicates the SRC2 protein where NR boxes 2 and 3 have been mutated from L*XX*LL to L*XX*AA. *D*, competition for binding of SRC2 by NR box peptides during a pull down of SRC2 by the GST fusion of the AR-LBD.

AF-1 and AF-2 are balanced in DU145 cells, and AF-2 dominates in HeLa cells (35, 36). Thus, our results are consistent with the notion that AR AF-2 is potent (35, 36) and contradict the notion that AR AF-2 has little or no intrinsic activity.

Mutation of individual SRC-2 NR boxes to L*XX*AA reveals a requirement for boxes 1 and 3 to provide full AR AF-2 activity, both in HeLa (Supplemental Fig. S1) and in DU145 cells (Fig. 2*B*). In contrast, NR box 2 of SRC2 is required to mediate TRβ AF-2 in HeLa (Supplemental Fig. S1), consistent with our own determinations of the affinity of SRC2 NR boxes for TRβ and with previous results (8, 28). Moreover, each mutant SRC showed equivalent ability to enhance activity of CBP AD2, which binds the SRCs at a distinct locus and in a manner that is independent of NR boxes (Supplemental Fig. S1) (8). Thus, the NR box mutations that reduce AR transactivation do not affect other elements of SRC2 activity.

NR boxes also played a role in the ability of SRC2 to coactivate full-length AR (Fig. 2*C*). For these experiments, we utilized an MMTV-LTR-driven reporter, because the N-C interaction is dispensable for optimal AR activity at this promoter, and HeLa cells, because AR AF-2 activity is relatively strong in this cell type. Here, SRC-2 enhancement of AR signaling was lessened when the NR boxes were mutated (17–19, 37). In particular, mutation of the third NR box (SRC2-3) abrogated SRC-2 action (see Fig. 4). Thus, there is exact congruence between the affinity of particular NR boxes for AR and their requirement for transactivation in the context of the isolated AR-LBD and full-length AR.

X-Ray Structures of AR-LBD in Complex with Coregulator Peptides Reveal the Atomic Basis for AR Selective Binding to SRC2 NR Boxes and ARA70—To determine how AR binds aromatic-rich coactivator domains and a particular subset of SRC NR boxes, we obtained crystal structures of the AR-LBD in complex with ARA70–2, SRC2-2, SRC2-3, and SRC3-2. As expected by analogy with other NR AF-2s, SRC2-3, SRC3-2, and ARA70 peptides bind as a short α-helix into the L-shaped hydrophobic cleft normally utilized by coactivators. On the contrary, the low affinity peptide SRC2-2 was seen to bind to AR-LBD AF through an energetically non-favorable conformation that could not be modeled as an α-helix. Comparison of the structures also reveals features that explain the ability of the AR AF-2 to bind to both L*XX*LL and F*XX*LF motifs.

The AR-LBD crystal structure in complex with the SRC2-3 peptide KENALLRYLLDKDD (14-mer) has been solved to 2.07 Å resolution. Thirteen residues of this peptide are clearly defined in the electron density, and the interaction buries 1322 Å^2 of predominantly hydrophobic surface area from both molecules. Our structure shows that SRC2-3 hydrophobic motif binds in nearly the same manner as previously stated in other NRs with L*XX*LL p160 coactivator motifs (32, 38–40). The residues located N-terminally from the first Leu residue (residue +1) are termed −1, −2, and so on, whereas the residues C-terminal from Leu+1, are termed +2, +3, etc. The core hydrophobic motif of the peptide (residues +1 to +5) forms a short α-helix that binds in the groove formed by helices 3, 4, 5, and 12. The LBD interacts primarily with the hydrophobic face of the SRC2-3 peptide α-helix formed by the side chains of the three L*XX*LL motif leucines (Leu-923, Leu-926, and Leu-927). The side chain of Leu-923 is embedded within the groove and forms van der Waals contacts with the side chains of Val-716, Met-734, and Asn-738. The side chain of Leu-927 is also isolated within the groove and makes van der Waals contacts with the side chains of Gln-733 and Met-734. The side chain of the second NR box 3 leucine (Leu-926), makes van der Waals contacts with the side chains of Val-716 and Met-894. The LBD residues implicated in hydrophobic contacts with the peptide are valines 716, 730, and 901, methionines 734 and 894, glutamines 733 and 738, Ile-898, and the non-polar parts of Asp-731 and Glu-893 and Glu-897.

The main-chain carbonyl groups of residues Leu-927, Asp-

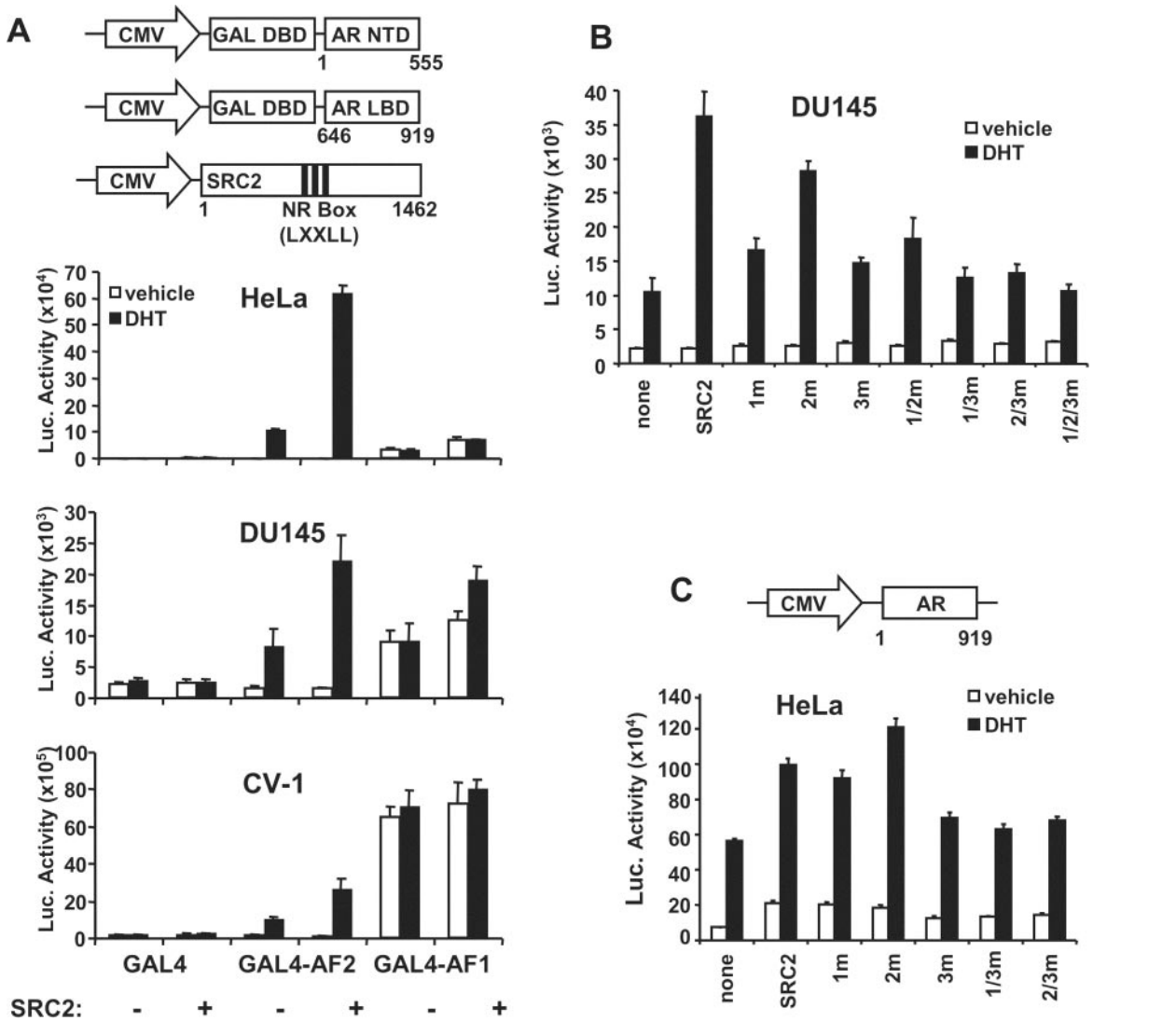

FIG. 2. **Transcriptional activation by AR, AR-NTD, and AR-LBD constructs and the enhancement of activation by SRC constructs.** *A*, transcriptional activation of a GAL4-luciferase reporter construct by fusions of GAL4 DNA binding domain with AR-NTD AF-1 or LBD AF-2 domains in three cell lines. In all cell lines, AR-LBD induces signaling in response to DHT, and this effect is enhanced by expression of SRC2. The level of AR-NTD-driven expression varies from cell line to cell line but remains constant in the presence or absence of both DHT and SRC2. *B*, the effects of mutation of SRC2 NR boxes 1 through 3 upon signaling by GAL4-AR-LBD constructs from a GAL-driven luciferase reporter. Mutations of SRC2-1 and SRC2-3 both significantly reduce potentiation of transactivation by AR. These mutational effects correlate with the observed relative affinities of the NR boxes for the receptor. *C*, activation of transcription at an MMTV-luciferase reporter by full-length AR and the effects of coexpression of SRC2 and mutants. Mutation of SRC2-3 significantly reduces potentiation of transactivation by AR.

930 and Asp-931 from the SRC2-3 peptide also interact with Lys-720, which is highly conserved in NRs and comprises the upper part of a charge clamp that stabilizes the α-helical NR box peptide conformation. However, contrary to predictions made on the basis of mutagenic analysis of AR surface residues (30), and comparisons with a glucocorticoid receptor/SRC2-3 structure (39), the SRC2-3 peptide does not form any hydrogen bonds to the second highly conserved charge clamp residue, Glu-897 on Helix 12. Instead, the peptide engages in hydrophobic contacts with Glu-897, and the distance to the three unpaired amide NH of the peptide helix is 5 Å, so electrostatic stabilization is possible. The peptide also engages in hydrogen bonding to seven water molecules in its vicinity. Residue Asp-928 located at position +6 adopts two different conformations. However, neither Asp-928 (+6) nor Arg-924 (+2) interact with charged residues on the AR surface that comprise a second charge clamp, again contrary to predictions made on the basis of a glucocorticoid receptor/SRC2-3 structure (39). Nonetheless, the SRC2-3 peptide displays clear electron density in the current structure for five residues N-terminal to the core hydrophobic motif and for four more residues C-terminal to the same motif, therefore displaying significantly greater electron density than any other NR box peptide in complex with a NR LBD to date.

The AR-LBD crystal structure in complex with the SRC3-2 peptide HKKLLQLLT (9-mer) has been solved to 2.7 Å resolution. All nine residues of this peptide are clearly defined in the electron density, and the interaction buries 1052 Å^2 of predominantly hydrophobic surface area from both molecules. Our structure shows that SRC3-2 hydrophobic motif binds in nearly the same manner as previously stated for SRC2-3. The LBD residues implicated in hydrophobic contacts with the peptide are valines 716 and 730, methionines 734 and 894, Ile-898, and the non-polar parts of Glu-897 and Lys-720, unexpectedly. SRC3-2 peptide is shorter C-terminally than SRC2-3 and does not make any hydrogen bonds with Lys-720. Surprisingly, another basic residue, Arg-726 adopts in this complex the C-terminal capping role stabilizing the peptide α-helix. This polar interaction is not present in the other peptide-AR-LBD complexes described in this report. This crystal structure shows

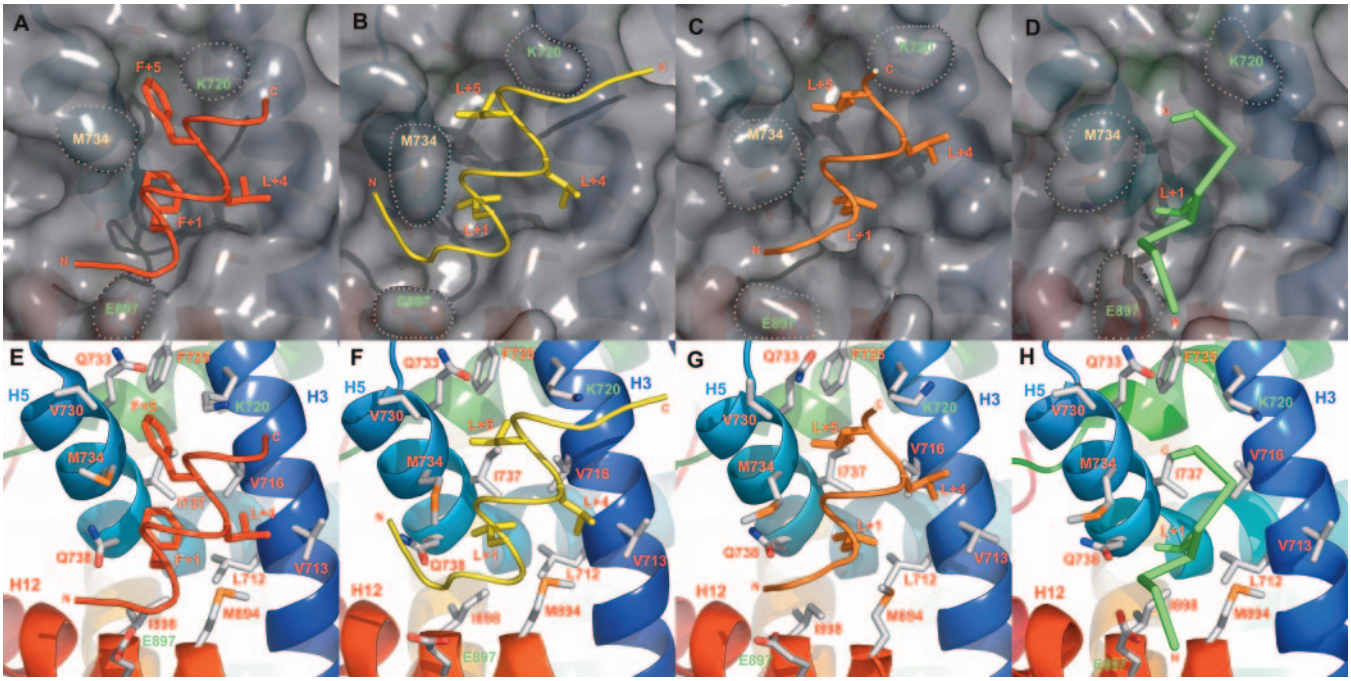

FIG. 3. **Associations of the AR-LBD with coactivator domains determined by x-ray crystallography (*A–H*).** Close-up views of the interaction between ARA70, SRC2-3, SRC2-2, and SRC3-2 peptides with AR-LBD AF2. The nuclear receptor AF-2 transactivation function is ascribed to a surface-exposed hydrophobic cleft comprising residues from helices 3 (*H3*, *dark blue*), 5 (*H5*, *pale blue*), and 12 (*H12*, *red*), as can be clearly seen in the *bottom figures* (*E–H*). *A–H*, the helix backbone of peptides from ARA70 (RETSEKFKLLFQSYN) (*left*, *red*), SRC2-3 (KENALLRYLLDKDD) (*middle left*, *yellow*), and SRC3-2 (HKKLLQLLT) (*middle right*, *orange*) are shown, and the non-helical SRC2-2 peptide backbone (KHKILHRLLQDSS) (*right*, *green*) can be seen. AR-LBD is represented by a solid semi-transparent surface (*gray*) in the *top figures* (*A–D*). The side chains of the motif hydrophobic residues Phe+1/Leu+1, Leu+4, and Phe+5/Leu+5 of the peptides are shown as *stick models*. Helix 12, with its Glu-897 side chain, stabilizes the N terminus of the ARA70 peptide, but not those of the SRC peptides. On H3, the side chain of Lys-720 is shown capping the C terminus of ARA70 and SRC2-3 peptides (*E* and *F*). *B*, the side chains of the AR-LBD residues contacting the peptides are depicted as *stick models*. ARA70: The triad compressed by the Phe aromatic side chains and Leu+4(F*XX*LF) fits tightly into a deep narrow pocket comprised of Val-716 and Val-730, Met-734, Ile-737, and the hydrophobic segment of Glu-893. The Leu side chains of SRC2-3 and SRC3-2 fit loosely into a flat hydrophobic pocket comprising the side chains of three valines, 716, 730, and 901, methionines 734 and 894, glutamines 733 and 738, Asp-731, and Glu-897. The accommodation of the bulkier Phe residues of ARA70 is accompanied by the rearrangements of Met-734, Glu-897, and Lys-720 predominantly (indicated by *gray dots* on the surface representation of AR). *D* and *H*, SRC2-2 does not bind to AR-LBD AF2 in an helical conformation, and, apart from Leu+1, the rest of the peptide cannot be superimposed to the other SRC peptides shown in this report. All the figures were generated with Pymol (42).

traceable electron density for six residues located at the protein N terminus that correspond to some residues of the hinge region of AR, and this is the first time that such residues are visible in an electron density. Those residues are in a random coiled-coil conformation.

The AR-LBD complex with the SRC2-2 peptide comprises the following sequence, KHKILHRLLQDSS (13-mer). Despite the fact that the crystal of SRC2-2 diffracted to 1.66 Å, the electron density that accounts for the peptide was more difficult to interpret and discontinuous suggesting that its affinity for AR-LBD is weak. It was surprising to state that SRC2-2 adopts two different conformations. The first was very similar to the SRC2-3 peptide and was modeled as a short α-helix. However, a second conformation, more similar to a coiled-coil, could be interpreted and refined (referred as the non-canonical conformation). In the SRC2-3-like conformation, interpretable electron density starts at the first leucine of the SRC2-2 peptide and finishes at Gln-928. Building this peptide from the box 3 conformation leaves only Leu-923 correctly placed within the weak electron density, His-924 bulges out of the density, and only the main chain returns to the electron density for Arg-925, Leu-926, Leu-927, and Gln-928. On the other hand, if NR box 2 is built and refined as a random coil, interpretable and continuous electron density starts at residue His-920 until Leu-926. From all these residues, only Leu-923 is completely defined, and for the rest of the six residues only the main chain is defined in the electron density, leaving the side chains unseen. NR box 2 in Box3-like conformation buries 850 Å^2 of predominantly hydrophobic surface area, whereas NR box 2 in random coil conformation buries 792 Å^2 of predominantly hydrophobic surface area from both molecules.

In the Box 3-like conformation, the side chain of Leu-923 is embedded within the groove and forms van der Waals contacts with the side chains of Leu-712, Asn-738, Met-894, and Ile-898. The side chain of Leu-927 makes van der Waals contacts with the side chain of Met-734. The side chain of the second NR box 2 leucine (Leu-926), makes van der Waals contacts with the side chain of Val-716. The LBD residues implicated in hydrophobic contacts with the peptide are Val-716, methionines 734 and 894, Gln-738, Ile-898, and the non-polar part of Glu-893. The residue Leu-926 interacts with *Lys-720*, through its main chain carbonyl group. In the non-canonical conformation, Leu-926 also interacts with *Lys-720*, through its main chain carbonyl group. NR box 2 peptide does not form any hydrogen bonds to the second highly conserved charge clamp residues, *Glu-897*, in either conformation. However, His-920 could be bonded to Glu-893. Except for three N-terminal residues that are disordered, the position and interactions of the ARA70 F*XX*LF peptide with the AR surface more closely recapitulate the binding mode observed in structures of ternary complexes of SRC L*XX*LL motifs with hormone-bound NR LBDs (Fig. 3, *A* and *C*) (32, 38–40). The triad of aromatic side chains (F*XX*LF) that forms the hydrophobic face of the coactivator helix fits tightly into a deep narrow pocket. In addition, charged residues at either end of the cleft, Glu-897 and Lys-720, cap the helix (the "charge clamp"). The fully engaged interaction is

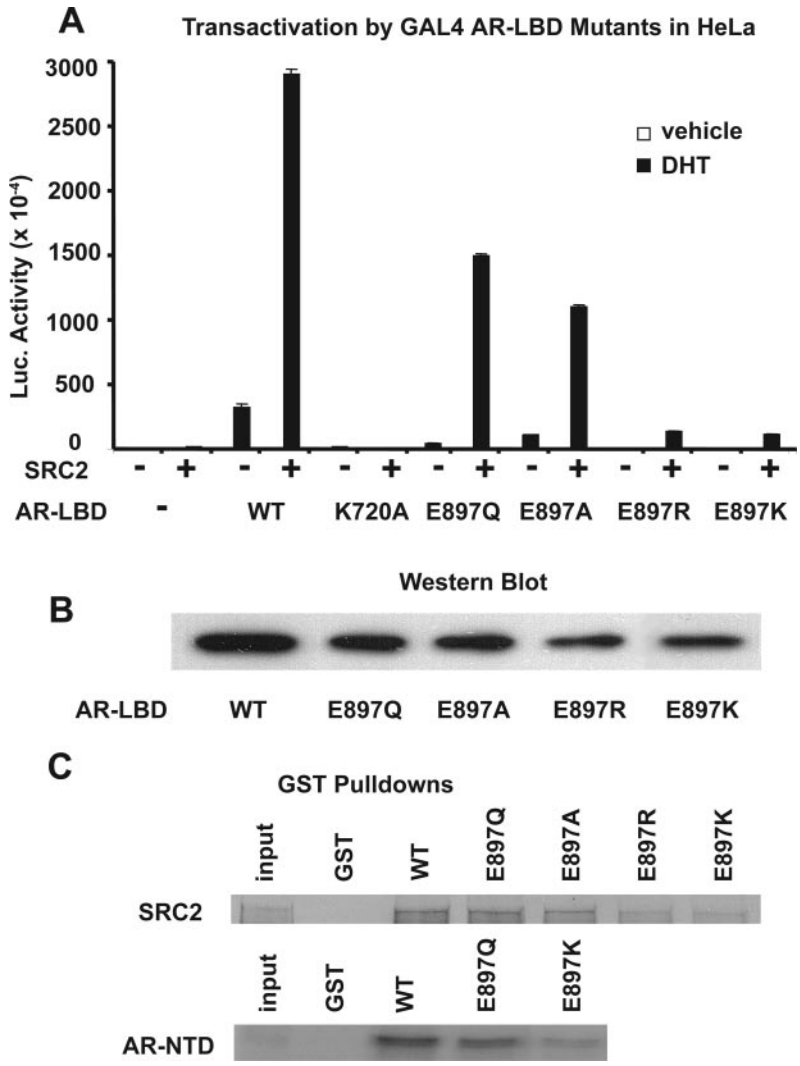

FIG. 4. **Role of the binding pocket and charge clamp residues of the AR-LBD AF-2 in interaction with cofactors and potentiation of transcriptional activation by a GAL4-AR-LBD construct.** *A*, removing the charge at Lys-720 or reversing the charge at Glu-897 (the positive and negative ends of the "charge clamp" that stabilizes helix dipole for the NR box) markedly reduces the potentiation of transcriptional activation by GAL AR-LBD by SRC2 in HeLa cells. However, neutralization of the charge at Glu-897 has modest effects on transcriptional activation. *B*, Western blot demonstrating that all Glu-897 mutants are expressed at similar levels in HeLa cells during the transactivation experiments. *C*, as expected from the peptide binding data (Fig. 1*A*), neutralization of charge at Glu-897 has no discernable effect upon the interaction of SRC2 as measured by GST Pull-down. Similarly, there is a modest reduction in binding of AR NTD by E897Q. However, reversal of charge (E897K) strongly reduces binding of both SRC2 and AR NTD.

manifested in the tight binding of this coactivator and its strong transactivation.

The AR-LBD Charge Clamp Plays Coregulator Selective Roles in Transactivation and Binding—One unexpected feature of our crystal structures is that the two residues that comprise the canonical AR-LBD charge clamp (Lys-720 on helix 3 and Glu-897 on helix 12) interact differently with F*XX*LF and L*XX*LL peptide backbones. Although previous studies suggested that Glu-897 was absolutely required for SRC binding, our structures revealed that Glu-897 is fully engaged with the carbamyl backbone of the F*XX*LF peptide, but not that of the L*XX*LL peptide. Similar arrangements were also observed in crystals of the AR-LBD in complex with artificial F*XX*LF and L*XX*LL peptides derived from phage display (41).

To understand the apparent discrepancy between the reported requirement for Glu-897 in AR activity and its lack of contact with the L*XX*LL motif of SRC2-3 in the crystal structure, we examined the effects of a series of charge clamp mutations on isolated AR AF-2 activity *in vivo* (Fig. 4*A*) and coregulator binding *in vitro* (Fig. 1*A*). As expected, a mutation within the upper charge clamp residue (Lys-720 → Ala) inhibited AR AF-2 activity (Fig. 4*A*) and prevented the recruitment of SRC2(Fig. 4*C*). The reversal of the normal negative charge at Glu-897 by introduction of a positive charge (Glu-897 → Lys and Glu-897 → Arg) had the same effect, probably due to repulsion of the charged NR box (30, 35). However, AR-LBDs bearing mutations that neutralized or lessened electrostatic potential at Glu-897 (Glu-897 → Ala and Glu-897 → Gln) retained significant AF-2 activity, especially in the presence of SRC2 (Fig. 4*A*) (9). These same mutants had no discernable effects upon recruitment of SRC2 (Fig. 4*C*) and a modest effect on recruitment of the AR NTD. This is in keeping with the effects of the Glu-897 → Gln mutation on NR box peptide recruitment (Fig. 1*A*). Western blotting of cell extracts confirmed that these differences in transcriptional activity were not related to differential expression of the AR-LBD mutants. Thus, the lower charge clamp residue (Glu-897) is dispensable for SRC-2 binding but required for ARA70 binding, exactly paralleling the requirement for this residue observed in both of our crystal structures.

DISCUSSION

In this report, we examined the binding of AR AF-2 to a range of target motifs within potential AR coactivators, confirmed the functional consequence of these interactions, and determined how AR AF-2 binds selectively to particular motifs. Our results confirm that AR AF-2 recognizes F*XX*LF motifs derived from the AR NTD and ARA70 with moderate affinity (<40 μM) but also show that AR binds some L*XX*LL motifs, particularly SRC2-1 and SRC2-3, with higher affinity (<10 μM). The discovery that AR AF-2 binds strongly to selected L*XX*LL motifs is surprising, but several lines of evidence confirm the importance of these interactions. Thus, bacterially expressed AR-LBD binds SRC2 strongly, as compared with TRβ AF-2 and AR AF-1, and these interactions are dependent upon NR boxes. Moreover, isolated AR AF-2 activates tran-

scription relatively strongly and does so in a manner that is potentiated by SRC2 and dependent upon SRC2-1 and SRC2-3. Finally, SRC2 L*XX*LL motifs were required for coactivation of full-length AR; at least at the MMTV promoter. Thus, AR AF-2 binds F*XX*LF motifs, but can also make important contacts with a subset of coregulator L*XX*LL motifs. AR therefore has the potential to activate transcription in an analogous manner to other NRs.

To understand the unusual selectivity of AR AF-2 for target coactivator motifs, we solved the structures of the AR-LBD in complex with an F*XX*LF motif derived from ARA70 and both high affinity (SRC2-3) and low affinity (SRC2-2) AR interacting motifs. Our structures indicate that the ARA70 F*XX*LF motif occupies a similar position to those of other coregulator NR box peptides in complex with LBDs of other NRs. Comparisons of each of the ternary complexes with each other, and with our own structures of AR in the absence of an associated peptide (not shown), reveal a striking rearrangement of the AF-2 surface that explains the ability of AR to accommodate the bulky hydrophobic side chains of the F*XX*LF motifs. Movements of Lys-720, Met-734, and Glu-897 create the deeper pockets and enhanced electrostatics allowing the binding of the ARA70 peptide (see Fig. 3). Similar rearrangements were also observed in crystals of AR-LBD in complex with artificial F*XX*LF and L*XX*LL peptides derived from phage display (41). Of these residues, Met-734 is relatively unique among the NR superfamily, and only conserved at an equivalent position within the glucocorticoid receptor LBD. Thus, the presence of Met-734 probably explains the unique capacity of the AR AF-2 surface to bind accommodate motifs with bulky hydrophobic side chains.

Crystal structures of AR-LBD in complex with SRC2-3 and SRC2-3 suggest an alternate explanation for the ability of AR AF-2 to discriminate between different L*XX*LL motifs. The SRC2-3 and SRC2-2 L*XX*LL motifs, by contrast to the ARA70 F*XX*LF motif and a variety of NR box peptides in complex with a variety of NR LBDs, are translated by about 2 Å in the cleft, toward helix 3. Overall, this unusual positioning disrupts the electrostatic stabilization characteristic of most NR/NR box interactions, likely explaining reduced AR binding to most L*XX*LL motifs. However, for SRC2-3, the high degree of negative charge in the four residues following the motif (sequence DKDD) interacts with positively charged patches on the receptor surface. In fact, these portions of the structure are better ordered than in all previous NR-coactivator complexes and are not visible in AR-LBD structures with the SRC2-2 peptide, which binds the AR-LBD with lower affinity. This influence offsets suboptimal electrostatics and explains the selective binding of AR AF-2 to SRC2-3. Thus, AR discriminates between cofactor NR box motifs by making auxiliary contacts outside of the core L*XX*LL motif. Interestingly, the ARA70 peptide is also relatively well ordered, about 12 of 15 amino acids are visible in our crystal structure. Although it has been previously suggested that NR LBDs may discriminate between target motifs by contacting residues that flank the hydrophobic L*XX*LL core (28, 31), our studies provide the first description of a structural basis for this effect.

AR AF-2 has the potential to participate in transcriptional activation in several ways, but the relative importance of different modes of AR AF-2 action are not yet clear. The N-C interaction is required for optimal AR action at a variety of androgen-regulated promoters, including those of prostate-specific genes such as *PSA* and *probasin*, suggesting that AF-2 mediates intramolecular interactions in these contexts. We predict that AR AF-2 could participate in coactivator binding in several contexts, including in the presence AR specific coactivators that contain F*XX*LF motifs, in conditions of SRC2 overexpression, and at promoters that resemble the MMTV-LTR. The requirement for AR AF-2 in growth of prostate cancer cells has not been rigorously addressed, but it is interesting to note that SRC2 enhancement of the androgen-dependent G_1 to S transition in LNCaP prostate tumor cells is dependent upon the integrity of the SRC2 NR box region (which binds AF-2) and independent of the SRC2 C terminus (which binds AR AF-1) (10). Perhaps AR AF-2 contacts with SRC L*XX*LL motifs will prove to be relevant for cell cycle progression.

In conclusion, AR has a potent AF-2 that drives the cell's expression program by binding F*XX*LF motifs and selected L*XX*LL motifs. The receptor uses the same general coactivator binding mechanisms as other NRs, by providing a dimorphic cleft that facilitates interaction with aromatic amino acids in addition to leucines. The ability of the AR surface to rearrange to interact with F*XX*LF motifs is unique among transcription factors and represents a gain of function relative to other structurally defined interactions in the family. Most NRs are unable to accommodate bulky side chains in the binding domains of the coactivators, and the dyadic recognition of AR has enabled development of more complex control mechanisms involving the NTD and the use of specialized subsets of coactivators. Most importantly, the new function *does not* come at the cost of a loss of ability to interact productively with SRCs. AR AF-2 interactions with SRCs are likely to be physiologically relevant, particularly in certain forms of prostate cancer.

Acknowledgments—We thank Eugene Hur, Luke M. Rice, Elena Sablin, and Maia Vinogradova for useful discussions and James Holton, Corie Ralston, and Advanced Light Source beamline staff for assistance in data collection and processing.

REFERENCES

1. Lee, H. J., and Chang, C. (2003) *Cell Mol. Life Sci.* **60,** 1613–1622
2. Liu, P. Y., Death, A. K., and Handelsman, D. J. (2003) *Endocr. Rev.* **24,** 313–340
3. Legros, J. J., Charlier, C., Bouillon, G., and Plomteux, G. (2003) *Ann. Endocrinol.* (*Paris*) **64,** 136
4. Gregory, C. W., He, B., Johnson, R. T., Ford, O. H., Mohler, J. L., French, F. S., and Wilson, E. M. (2001) *Cancer Res.* **61,** 4315–4319
5. Culig, Z., Klocker, H., Bartsch, G., and Hobisch, A. (2002) *Endocr. Relat. Cancer* **9,** 155–170
6. Santos, A. F., Huang, H., and Tindall, D. J. (2004) *Steroids* **69,** 79–85
7. Balk, S. P. (2002) *Urology* **60,** 132–138; discussion 138–139
8. Ding, X. F., Anderson, C. M., Ma, H., Hong, H., Uht, R. M., Kushner, P. J., and Stallcup, M. R. (1998) *Mol. Endocrinol.* **12,** 302–313
9. Berrevoets, C. A., Doesburg, P., Steketee, K., Trapman, J., and Brinkmann, A. O. (1998) *Mol. Endocrinol.* **12,** 1172–1183
10. Shang, Y., Myers, M., and Brown, M. (2002) *Mol. Cell* **9,** 601–610
11. Gregory, C. W., Fei, X., Ponguta, L. A., He, B., Bill, H. M., French, F. S., and Wilson, E. M. (2004) *J. Biol. Chem.* **279,** 7119–7130
12. Blaszczyk, N., Masri, B. A., Mawji, N. R., Ueda, T., McAlinden, G., Duncan, C. P., Bruchovsky, N., Schweikert, H. U., Schnabel, D., Jones, E. C., and Sadar, M. D. (2004) *Clin. Cancer Res.* **10,** 1860–1869
13. Needham, M., Raines, S., McPheat, J., Stacey, C., Ellston, J., Hoare, S., and Parker, M. (2000) *J. Steroid Biochem. Mol. Biol.* **72,** 35–46
14. Leo, C., and Chen, J. D. (2000) *Gene* (*Amst.*) **245,** 1–11
15. Alen, P., Claessens, F., Schoenmakers, E., Swinnen, J. V., Verhoeven, G., Rombauts, W., and Peeters, B. (1999) *Mol. Endocrinol.* **13,** 117–128
16. He, B., Lee, L. W., Minges, J. T., and Wilson, E. M. (2002) *J. Biol. Chem.* **277,** 25631–25639
17. Ma, H., Hong, H., Huang, S. M., Irvine, R. A., Webb, P., Kushner, P. J., Coetzee, G. A., and Stallcup, M. R. (1999) *Mol. Cell. Biol.* **19,** 6164–6173
18. Christiaens, V., Bevan, C. L., Callewaert, L., Haelens, A., Verrijdt, G., Rombauts, W., and Claessens, F. (2002) *J. Biol. Chem.* **277,** 49230–49237
19. Powell, S. M., Christiaens, V., Voulgaraki, D., Waxman, J., Claessens, F., and Bevan, C. L. (2004) *Endocr. Relat. Cancer* **11,** 117–130
20. He, B., Minges, J. T., Lee, L. W., and Wilson, E. M. (2002) *J. Biol. Chem.* **277,** 10226–10235
21. He, B., and Wilson, E. M. (2002) *Mol. Genet. Metab.* **75,** 293–298
22. Zhou, Z. X., He, B., Hall, S. H., Wilson, E. M., and French, F. S. (2002) *Mol. Endocrinol.* **16,** 287–300
23. He, B., Kemppainen, J. A., and Wilson, E. M. (2000) *J. Biol. Chem.* **275,** 22986–22994
24. Matias, P. M., Donner, P., Coelho, R., Thomaz, M., Peixoto, C., Macedo, S., Otto, N., Joschko, S., Scholz, P., Wegg, A., Basler, S., Schafer, M., Egner, U., and Carrondo, M. A. (2000) *J. Biol. Chem.* **275,** 26164–26171
25. Holton, J., and Alber, T. (2004) *Proc. Natl. Acad. Sci. U. S. A.* **101,** 1537–1542
26. Brunger, A. T., Adams, P. D., and Rice, L. M. (1998) *Curr. Opin. Struct. Biol.* **8,** 606–611
27. Engh, R. A., and Huber, R. (1991) *Acta Crystallogr. Sect. A* **47,** 392–400
28. Darimont, B. D., Wagner, R. L., Apriletti, J. W., Stallcup, M. R., Kushner, P. J.,

Baxter, J. D., Fletterick, R. J., and Yamamoto, K. R. (1998) *Genes Dev.* **12,** 3343–3356
29. Bourguet, W., Andry, V., Iltis, C., Klaholz, B., Potier, N., Van Dorsselaer, A., Chambon, P., Gronemeyer, H., and Moras, D. (2000) *Protein Expression Purif.* **19,** 284–288
30. He, B., and Wilson, E. M. (2003) *Mol. Cell. Biol.* **23,** 2135–2150
31. McInerney, E. M., Rose, D. W., Flynn, S. E., Westin, S., Mullen, T. M., Krones, A., Inostroza, J., Torchia, J., Nolte, R. T., Assa-Munt, N., Milburn, M. V., Glass, C. K., and Rosenfeld, M. G. (1998) *Genes Dev.* **12,** 3357–3368
32. Shiau, A. K., Barstad, D., Loria, P. M., Cheng, L., Kushner, P. J., Agard, D. A., and Greene, G. L. (1998) *Cell* **95,** 927–937
33. Ribeiro, R. C., Apriletti, J. W., West, B. L., Wagner, R. L., Fletterick, R. J., Schaufele, F., and Baxter, J. D. (1995) *Ann. N. Y. Acad. Sci.* **758,** 366–389
34. Moore, J. M., Galicia, S. J., McReynolds, A. C., Nguyen, N. H., Scanlan, T. S., and Guy, R. K. (2004) *J. Biol. Chem.* **279,** 27584–27590
35. Slagsvold, T., Kraus, I., Bentzen, T., Palvimo, J., and Saatcioglu, F. (2000) *Mol. Endocrinol.* **14,** 1603–1617
36. Wang, Q., Lu, J., and Yong, E. L. (2001) *J. Biol. Chem.* **276,** 7493–7499
37. Bevan, C. L., Hoare, S., Claessens, F., Heery, D. M., and Parker, M. G. (1999) *Mol. Cell. Biol.* **19,** 8383–8392
38. Shiau, A. K., Barstad, D., Radek, J. T., Meyers, M. J., Nettles, K. W., Katzenellenbogen, B. S., Katzenellenbogen, J. A., Agard, D. A., and Greene, G. L. (2002) *Nat. Struct. Biol.* **9,** 359–364
39. Bledsoe, R. K., Montana, V. G., Stanley, T. B., Delves, C. J., Apolito, C. J., McKee, D. D., Consler, T. G., Parks, D. J., Stewart, E. L., Willson, T. M., Lambert, M. H., Moore, J. T., Pearce, K. H., and Xu, H. E. (2002) *Cell* **110,** 93–105
40. Pike, J. W., Yamamoto, H., and Shevde, N. K. (2002) *Adv. Ren. Replace Ther.* **9,** 168–174
41. Hur, E., Pfaff, S. J., Payne, E. S., Gron, H., Buehrer, B. M., and Fletterick, R. J. (2004) *PLoS Biol.* **2,** E274
42. DeLano, W. L. (2002) *Pymol*, DeLano Scientific, San Carlos, CA